Progress In Electromagnetics Research Letters, Vol. 28, 149–158, 2012

ANALYTIC AND NUMERICALLY EFFICIENT SCATTERING EQUATIONS FOR AN INFINITELY FLANGED COAXIAL LINE

Y. H. Cho*

School of Information and Communication Engineering, Mokwon University, 21 Mokwon St., Seo-gu, Daejeon 302-729, Republic of Korea

Abstract—An infinitely flanged coaxial line is analytically solved with the mode-matching technique and Green's function to propose a precise yet fast-convergent scattering solution for complex permittivity measurement. Based on virtual current cancelation, we formulate the open half-space fields in terms of coaxial modes and related Green's functions and thus obtain the simultaneous equations with rapidly convergent integrals. Numerical computations were performed in terms of reflection coefficients and radiation patterns.

1. INTRODUCTION

A flanged coaxial line has been extensively studied to obtain material characteristics for biological substances [1], non-destructive test [2], resonant dielectric absorption [3], permittivity determination [4], moisture layers [5], agricultural products [6], IC packages [7], and concrete [8]. Even though the applications for material measurements are somewhat different, the basic idea is very similar one another [1–8]. Measuring the reflection coefficients with a fixed probe is utilized to determine the complex permittivity of an unknown material. We usually perform iteration procedures to reduce errors between pre-obtained measurement results and simulations with various complex permittivity.

As a result, the analytic formulations of scattering phenomena for probe and material are very important to estimate material characteristics. To obtain precise scattering equations, a variety of

Received 9 November 2011, Accepted 16 December 2011, Scheduled 20 December 2011

* Corresponding author: Yong Heui Cho (yongheuicho@gmail.com).

numerical methods have been proposed [9–16]. The Wiener-Hopf method and unilateral Fourier transform [9] were applied to a problem of radiation from a coaxial line with an infinite flange and thick inner conductor. A quasi-static analysis [10] was proposed to get an approximate closed-form solution. The Hankel transform and mode-matching technique [11–13] allow us to formulate the scattered fields in analytic representations. However, the radiation integrals in [11–13] have singularities and oscillating behaviors, thus indicating that the proposed integrals are complicated to deduce and inefficient for numerical computations. In [14, 15], the authors used versatile numerical algorithms such as the boundary integral equation [14] and the two-dimensional finite-difference frequency-domain method [15], respectively. Recently, by using the Sommerfeld identity similar to the Hankel transform, an approximate but efficient exponential series solution was given in [16] based on the matrix pencil method. The analytic method based on the eigenfunctions satisfying the edge condition was also used in [18, 19]. Even though the method in [18] is analytic, the radiation integrals in [18] still have several singular points which make numerical integrations difficult.

The aim of this work is to show an alternative method based on the mode-matching technique and Green's function. The Green's function approach combined with virtual current cancellation [17] and integral path deforming also yields a fast-convergent radiation integral that is free of singularity and very efficient for numerical integration. In the following Section, we extend the methodology proposed in [17] to the problem of a flanged coaxial line.

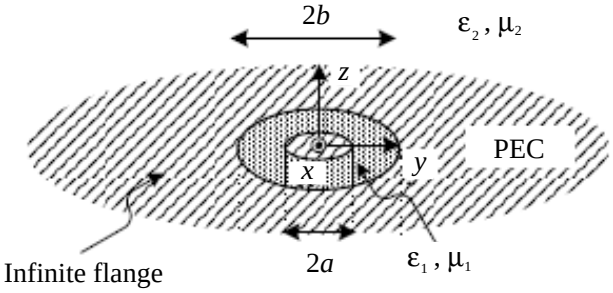

Figure 1. Geometry of an infinitely flanged coaxial line.

2. FIELD REPRESENTATION AND ANALYSIS

Consider the TM_{0s} mode propagates through a coaxial line shown in Figure 1 and is reflected at the end of a coaxial line ($z = 0$). Note that s represents the mode number of an incident wave. The coaxial line is truncated at $z = 0$ and connected to a perfectly conducting infinite flange at $z = 0$. Due to the geometric discontinuity at $z = 0$, the infinite number of guided waves are generated in region (I) ($z \leq 0$) and some incident power is transmitted into the free-space that is denoted as region (II) ($z > 0$). We select the time convention as $e^{-i\omega t}$ which is suppressed throughout. The incident and reflected electric fields E_ρ are conveniently defined as

$$E_\rho^i(\rho, z) = -\eta_1 \kappa_s C_0'(\kappa_s \rho) e^{i\xi_s z} \tag{1}$$

$$E_\rho^r(\rho, z) = -\eta_1 \kappa_s C_0'(\kappa_s \rho) e^{-i\xi_s z}, \tag{2}$$

where $\rho = \sqrt{x^2 + y^2}$, $\eta_1 = \sqrt{\mu_1/\epsilon_1}$, $\xi_m = \sqrt{k_1^2 - \kappa_m^2}$, $k_1 = \omega\sqrt{\mu_1 \epsilon_1}$, $(\cdot)'$ denotes differentiation with respect to the argument,

$$C_0(\kappa_m \rho) = \begin{cases} J_0(\kappa_m \rho) N_0(\kappa_m b) - N_0(\kappa_m \rho) J_0(\kappa_m b) & (m \neq 0) \\ \frac{2}{\pi} \log \frac{b}{\rho} & (m = 0) \end{cases}, \tag{3}$$

$J_0(\cdot)$ and $N_0(\cdot)$ are the zeroth-order Bessel functions of the first and second kinds, respectively, $\kappa_0 = 0$, and κ_m is determined by equating $C_0(\kappa_m a) = 0$ $(m = 1, 2, \ldots)$. A coaxial function $C_0(\kappa_m \rho)$ satisfies the Bessel's differential equation as

$$\left[\frac{1}{\rho}\frac{d}{d\rho}\left(\rho \frac{d}{d\rho}\right) + \kappa_m^2\right] C_0(\kappa_m \rho) = 0. \tag{4}$$

When $s = 0$, (1) denotes a TEM mode. The incident E_ρ^i field is scattered at the boundary at $z = 0$. Based on the Fourier-Bessel series, the magnetic vector potential A_z^I in region (I) ($z < 0$) is formulated to represent the scattered fields as

$$A_z^I(\rho, z) = \mu_1 \sum_{m=0}^{\infty} p_m C_0(\kappa_m \rho) e^{-i\xi_m z}, \tag{5}$$

where p_m are the unknown modal coefficients to be determined with simultaneous equations that will be shown in (20). The electric field in region (I) $E_\rho^I(\rho, z)$ can be obtained with $E_\rho^I(\rho, z) = \frac{i}{\omega \mu_1 \epsilon_1} \frac{\partial^2}{\partial z \partial \rho} A_z^I(\rho, z)$. In terms of the Sturm-Liouville theory, the eigenfunctions $C_0(\kappa_m \rho)$ are orthogonal each other and constitute a complete basis set for region (I). Therefore, we can consider p_m the expansion coefficients for the Fourier-Bessel series.

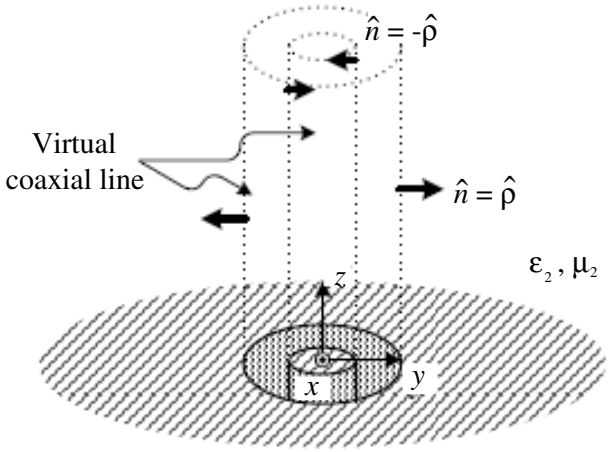

Figure 2. Artificial geometry for virtual current cancellation.

The magnetic vector potential A_z^{II} in open half-space region ($z > 0$) can be obtained based on virtual current cancelation. Even though virtual currents induced on a virtual coaxial line at $\rho = a$, b and $z > 0$ illustrated in Figure 2 are artificial, this concept facilitates the simplified yet precise field representations in open region. It should be noted that we assume the virtual coaxial line at $\rho = a$, b and $z > 0$ to be made of PEC (Perfect Electric Conductor). Since a virtual coaxial line is introduced in open region ($z > 0$), we can easily match the potential $E_m(\rho, z)$ ($z > 0$) for the virtual coaxial line and $A_z^I(\rho, z)$ ($z < 0$) by a standard mode-matching technique. In the next step, the component $R_m^E(\rho, z)$ is generated to remove the inevitable discontinuities at $\rho = a$ and b caused by a virtual coaxial line. By this basic concept of virtual current cancelation, we can formulate the magnetic vector potential A_z^{II} for open half-space region ($z > 0$) as

$$A_z^{II}(\rho, z) = \mu_2 \sum_{m=0}^{\infty} r_m \left[E_m(\rho, z) + R_m^E(\rho, z) \right], \tag{6}$$

where r_m are the unknown modal coefficients for region (II),

$$E_m(\rho, z) = C_0(\kappa_m \rho) \frac{e^{i\eta_m z}}{i\eta_m}, \tag{7}$$

$\eta_m = \sqrt{k_2^2 - \kappa_m^2}$, and $k_2 = \omega\sqrt{\mu_2 \epsilon_2}$. In order to determine the coefficients r_m, the normal electric field continuity $\partial E_z/\partial z - \rho_e/\epsilon$ at $z = 0$ should be utilized. The z-directed electric field E_z is represented

as $E_z(\rho,z)=\frac{i}{\omega\mu\epsilon}(\frac{\partial^2}{\partial z^2}+k^2)A_z^I(\rho,z)$. Enforcing the normal electric field continuity at $z=0$, we get

$$r_m=-\frac{\epsilon_2}{\epsilon_1}i\xi_m p_m. \tag{8}$$

where we assume $\partial/\partial z R_m^E(\rho,z)|_{z=0}=0$. Note that the condition $\partial/\partial z R_m^E(\rho,z)|_{z=0}=0$ will be verified later.

In terms of the Green's function relation, the component $R_m^E(\rho,z)$ to cancel out $E_m(\rho,z)$ is formulated as

$$R_m^E(\rho,z)=-\int\frac{\partial}{\partial n'}\left[E_m(\bar{r}')\right]G_A^{zz}(\bar{r},\bar{r}')d\bar{r}', \tag{9}$$

where n is an outward normal direction denoted in Figure 2 and $G_A^{zz}(\bar{r},\bar{r}')$ is the z-directional Green's function excited by the z-directed source in terms of a magnetic vector potential A. Substituting (7) into (9) yields

$$R_m^E(\rho,z)=-\frac{2i}{\pi}\int_0^\infty\frac{\cos(\zeta z)}{\kappa^2-\kappa_m^2}\left[\frac{J_0(\kappa_m b)}{J_0(\kappa_m a)}f_E(\rho,a;\kappa)-f_E(\rho,b;\kappa)\right]d\zeta, \tag{10}$$

where $\kappa=\sqrt{k_2^2-\zeta^2}$ and

$$f_E(\rho,\rho';\kappa)=\begin{cases}J_0(\kappa\rho')H_0^{(1)}(\kappa\rho) & \text{for } \rho>\rho'\\ J_0(\kappa\rho)H_0^{(1)}(\kappa\rho') & \text{for } \rho<\rho'\end{cases}. \tag{11}$$

Since (10) has singular points at $\kappa=\pm\kappa_m$, (10) is not efficient for numerical computations. As such, we use the integral path deformation proposed in [17]. According to [17], we replace ζ with $\zeta=k_2v(v-i)$. Then,

$$\begin{aligned}R_m^E(\rho,z) &= -\frac{2k_2i}{\pi}\int_0^\infty\frac{(2v-i)\cos(\zeta z)}{\kappa^2-\kappa_m^2}\\ &\quad\times\left[\frac{J_0(\kappa_m b)}{J_0(\kappa_m a)}f_E(\rho,a;\kappa)-f_E(\rho,b;\kappa)\right]dv.\end{aligned} \tag{12}$$

Considering (12), we can prove $\partial/\partial z R_m^E(\rho,z)|_{z=0}=0$. Although the integrand in (12) is oscillating when $v\gg1$ and $z\gg1$, the integrand does not have any singularities. Thus, we can integrate (12) very easily to get the magnetic vector potential A_z^{II} in (6) for the open region near $z\approx0$.

Using the Green's second integral identity, the magnetic vector potential $A_z^{II}(\rho,z)$ in (6) is also simplified to a finite integral as

$$E_m(\rho,z)+R_m^E(\rho,z)=-\int_a^b C_0(\kappa_m\rho')K_{\rho z}(\rho')\rho'd\rho'+\Delta_0(\rho,z), \tag{13}$$

where $r = \sqrt{\rho^2 + z^2}$, $\theta = \cos^{-1}(z/r)$,

$$K_{\rho z}(\rho') = \int_0^{2\pi} \frac{e^{ik_2 R_0}}{2\pi R_0} d\phi' = i \int_0^{\infty} f_E(\rho, \rho'; \kappa) \cos(\zeta z) d\zeta \quad (14)$$

$$R_0 = \sqrt{r^2 - 2\rho\rho' \cos\phi' + (\rho')^2} \quad (15)$$

$$\Delta_0(\rho, z) = \delta_{m0} \frac{i2k_2 a}{\pi} \log\left(\frac{b}{a}\right) \times \int_0^{\infty} \frac{(2v - i)}{\kappa^2} \cos(\zeta z) \frac{\partial}{\partial \rho'} f_E(\rho, \rho'; \kappa)\Big|_{\rho'=a} dv, \quad (16)$$

and δ_{ml} is the Kronecker delta. When we adopt the spherical coordinate system (r, θ, ϕ) and $r \to \infty$, the far-field for the magnetic vector potential $A_z^{II}(\rho, z)$ in (6) is asymptotically given by

$$A_z^{II}(r, \theta) \sim \mu_2 \frac{\epsilon_2}{\epsilon_1} \frac{ie^{ik_2 r}}{r} \sum_{m=0}^{\infty} p_m \xi_m \left[F_0^{cx}(\kappa_m, k_2 \sin\theta) + \delta_{m0} \frac{2a}{\pi} \log\left(\frac{b}{a}\right) \frac{J_1(k_2 \sin\theta)}{k_2 \sin\theta} \right], \quad (17)$$

where

$$F_0^{cx}(\kappa_m, \kappa) = \frac{2}{\pi(\kappa_m^2 - \kappa^2) J_0(\kappa_m a)} \times \left[J_0(\kappa_m a) J_0(\kappa b) - J_0(\kappa a) J_0(\kappa_m b) + \kappa a J_1(\kappa a) \log\left(\frac{b}{a}\right) \delta_{m0} \right]. \quad (18)$$

Similarly, the E_θ field in the far-field is represented as

$$E_\theta^{II}(r, \theta) \sim \eta_2 \frac{\epsilon_2}{\epsilon_1} \frac{e^{ik_2 r}}{r} k_2 \sin\theta \sum_{m=0}^{\infty} p_m \xi_m \left[F_0^{cx}(\kappa_m, k_2 \sin\theta) + \delta_{m0} \frac{2a}{\pi} \log\left(\frac{b}{a}\right) \frac{J_1(k_2 \sin\theta)}{k_2 \sin\theta} \right]. \quad (19)$$

Differentiating (5) and (6) with respect to the ρ-axis and applying the H_ϕ field continuity at $z = 0$ gives the final simultaneous equations for p_m as

$$\sum_{m=0}^{\infty} p_m I_E(m, l) = s_{E,l}, \quad (20)$$

where

$$I_E(m, l) = D_m \delta_{ml} + \frac{\epsilon_2}{\epsilon_1} i\xi_m \left[\frac{D_m}{i\eta_m} \delta_{ml} + I_{ml}^E \right] \quad (21)$$

$$s_{E,l} = -2D_s \delta_{sl} \quad (22)$$

$$D_m = \frac{2}{\pi^2}\left[1 - \frac{J_0^2(\kappa_m b)}{J_0^2(\kappa_m a)} + 2\log\left(\frac{b}{a}\right)\delta_{m0}\right] \quad (23)$$

$$I_{ml}^E = -\frac{2k_2\kappa_l i}{\pi}\int_0^\infty \frac{(2v-i)\kappa}{(\kappa^2-\kappa_m^2)(\kappa^2-\kappa_l^2)} \times\left[\frac{J_0(\kappa_m b)}{J_0(\kappa_m a)}J_0(\kappa a)f_l^E(a;\kappa) - H_0^{(1)}(\kappa b)f_l^E(b;\kappa)\right]dv \quad (24)$$

$$f_l^E(a;\kappa) = \kappa b H_0^{(1)}(\kappa b)C_0'(\kappa_l b) - \kappa a H_0^{(1)}(\kappa a)C_0'(\kappa_l a) \quad (25)$$

$$f_l^E(b;\kappa) = \kappa b J_0(\kappa b)C_0'(\kappa_l b) - \kappa a J_0(\kappa a)C_0'(\kappa_l a). \quad (26)$$

3. NUMERICAL COMPUTATIONS

We solved the simultaneous equations given by (20) and compared with [2, 16]. Figure 3 illustrates the behaviors of reflection coefficients when a TEM mode ($s = 0$) impinges on the flanged open end of a coaxial line. In this figure, M is the number of truncated modes. Our computational results based on (20) agree very well with [2, 16] when $M \geq 2$. A dominant mode solution ($M = 1$) is only valid for low frequency.

In Figure 4, we can observe the magnitude variations of the integrand for I_{ml}^E in (24). The radiation integral with deformed integral path I_{ml}^E does not have any singularity: this is desirable for numerical integration. Furthermore, the integrand shown in Figure 4 has fast-convergent characteristics when the integration variable v becomes

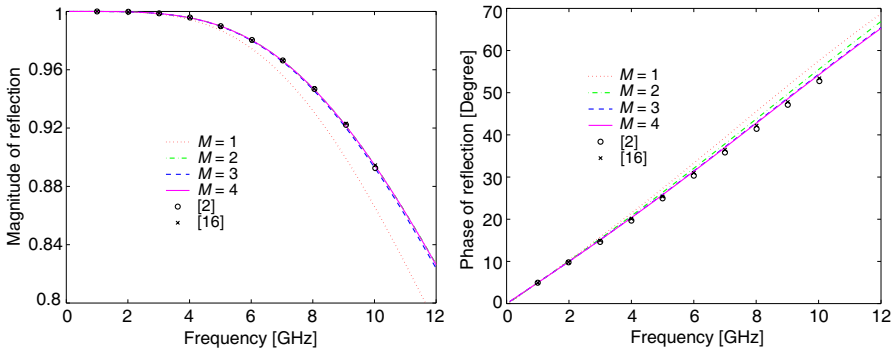

Figure 3. Behaviors of reflection coefficients (Γ) with $s = 0$ (TEM incidence), $a = 1.4364$ [mm], $b = 4.725$ [mm], $\epsilon_1 = \epsilon_2 = 2.05\epsilon_0$, and $\mu_1 = \mu_2 = \mu_0$. (a) Magnitude of Γ. (b) Phase of Γ.

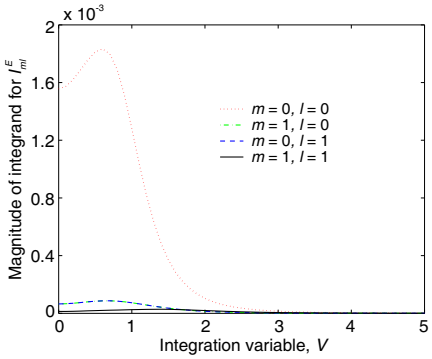

Figure 4. Variations of the integrand for I_{ml}^E versus an integration variable v with $f = 8$ [GHz] and the same parameters in Figure 3.

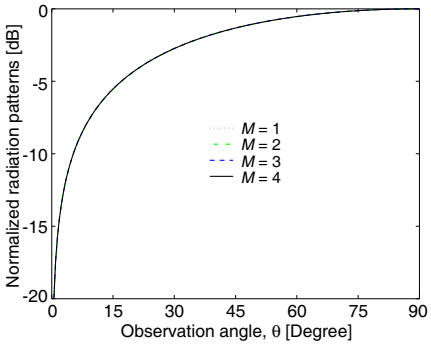

Figure 5. Behaviors of radiation patterns versus an observation angle θ with $f = 8$ [GHz] and the same parameters in Figure 3.

large. Our computational experience indicates that the maximum value of v for numerical integration can be five to ten in order to obtain numerical convergence for most of cases.

Figure 5 shows the behaviors of radiation patterns of a flanged coaxial line. Contrary to the reflection characteristics in Figure 3, a dominant mode solution ($M = 1$) is almost the same as the higher-mode solutions ($M \geq 2$). In addition, the radiation pattern of a flanged coaxial line has peak antenna gain at $\theta = 90^\circ$ which is similar to a flanged monopole antenna. This indicates that the reflection characteristics are mainly determined near the open end and flange of a coaxial line.

4. CONCLUSIONS

Using the Green's function and mode-matching technique, an analytic and numerically efficient analytic approach is proposed for an infinitely flanged coaxial line. The reflection behaviors of a flanged coaxial line were compared with other results and showed good agreements. The permittivity measurement and estimation with a flanged coaxial line can be more precisely performed with the proposed analytic solutions with fast-convergent radiation integrals.

REFERENCES

1. Stuchly, M. A. and S. S. Stuchly, "Coaxial line reflection method for measuring dielectric properties of biological substances at radio and microwave frequencies — A review," *IEEE Trans. Instrum. Meas.*, Vol. 29, No. 3, 176–183, Sep. 1980.
2. Mosig, J. R., J. E. Besson, M. Gex-Fabry, and F. E. Gardiol, "Reflection of an open-ended coaxial line and application to non-destructive measurement of materials," *IEEE Trans. Instrum. Meas.*, Vol. 30, No. 1, 46–51, Mar. 1981.
3. Foster, K. R., B. R. Epstein, and M. A. Gealt, "Resonances in the dielectric absorption of DNA?" *Biophysical Journal*, Vol. 52, No. 3, 421–425, Sep. 1987.
4. Zheng, H. and C. E. Smith, "Permittivity measurements using a short open-ended coaxial line probe," *IEEE Microwave Guided Wave Lett.*, Vol. 1, No. 11, 337–339, Nov. 1991.
5. Li, L. L., N. H. Ismail, L. S. Taylor, and C. C. Davis, "Flanged coaxial microwave probes for measuring thin moisture layers," *IEEE Trans. Biomed. Eng.*, Vol. 39, No. 1, 49–57, Jan. 1992.
6. Sheen, N. I. and I. M. Woodhead, "An open-ended coaxial probe for broad-band permittivity measurement of agricultural products," *J. Agr. Eng. Res.*, Vol. 74, No. 2, 193–202, Oct. 1999.
7. Ju, Y., M. Saka, and H. Abe, "Microwave nondestructive detection of delamination in IC packages utilizing open-ended coaxial line sensor," *NDT and E International*, Vol. 32, No. 5, 259–264, Jul. 1999.
8. Filali, B., F. Boone, J. Rhazi, and G. Ballivy, "Design and calibration of a large open-ended coaxial probe for the measurement of the dielectric properties of concrete," *IEEE Trans. Microwave Theory Tech.*, Vol. 56, No. 10, 2322–2328, Oct. 2008.
9. Zhurav, S. M., "TEM-wave radiation from a coaxial waveguide with an infinite flange," *Radiophysics and Quantum Electronics*, Vol. 20, No. 7, 752–755, 1977.
10. Misra, D. K., "A quasi-static analysis of open-ended coaxial lines," *IEEE Trans. Microwave Theory Tech.*, Vol. 35, No. 10, 925–928, Oct. 1987.
11. Lee, J. H., H. J. Eom, and K. H. Jun, "Reflection of a coaxial line radiating into a parallel plate," *IEEE Microwave Guided Wave Lett.*, Vol. 6, No. 3, 135–137, Mar. 1996.
12. Noh, Y. C. and H. J. Eom, "Radiation from a flanged coaxial line into a dielectric slab," *IEEE Trans. Microwave Theory Tech.*,

Vol. 47, No. 11, 2158–2161, Nov. 1999.

13. Panariello, G., L. Verolino, and G. Vitolo, "Efficient and accurate full-wave analysis of the open-ended coaxial cable," *IEEE Trans. Microwave Theory Tech.*, Vol. 49, No. 7, 1304–1309, Jul. 2001.
14. Asvestas, J. S., "Radiation of a coaxial line into a half-space," *IEEE Trans. Antennas Propagat.*, Vol. 54, No. 6, 1624–1631, Jun. 2006.
15. Huang, R. and D. Zhang, "Analysis of open-ended coaxial probes by using a two-dimensional finite-difference frequency-domain method," *IEEE Trans. Instrum. Meas.*, Vol. 57, No. 5, 931–939, May 2008.
16. Tan, W. and Z. Shen, "Efficient analysis of open-ended coaxial line using Sommerfeld identity and matrix pencil method," *IEEE Microw. Wireless Compon. Lett.*, Vol. 18, No. 1, 7–9, Jan. 2008.
17. Cho, Y. H., "TM plane-wave scattering from finite rectangular grooves in a conducting plane using overlapping T-block method," *IEEE Trans. Antennas Propagat.*, Vol. 54, No. 2, 746–749, Feb. 2006.
18. Serizawa, H. and K. Hongo, "Radiation from a flanged rectangular waveguide," *IEEE Trans. Antennas Propagat.*, Vol. 53, No. 12, 3953–3962, Dec. 2005.
19. Jia, H., K. Yasumoto, and K. Yoshitomi, "Analysis of rectangular groove waveguides using Fourier transform technique," *Microwave Optical Tech. Lett.*, Vol. 41, No. 5, 388–392, Jun. 2004.